Inward Melting Inside a Horizontal Multilobed Capsule with Conductive Wall Affected by Ag-MgO/Water Hybrid and MgO/Water Nanofluids

Mohammad Hassan Shojaeefard[a], Mahmoud Jourabian*,[a], Ahmad Ali Rabienataj Darzi[b] , Ali Bayat[c]

[a] School of Mechanical Engineering, Iran University of Science and Technology, Tehran, Iran.
[b] Department of Mechanical Engineering, University of Mazandaran, Babolsar, Mazandaran, Iran.
[c] Department of Civil Engineering, Islamic Azad University, Arak Branch, Arak, Markazi, Iran.

ABSTRACT

We scrutinize the possibility of boosting the functionality of an isothermally heated horizontal capsule filled with the phase change material (PCM) as the thermal energy storage (TES) system. There is the conjugate heat transfer at the wall. The constrained inward melting of the water/ice (Pr=6.2) at Ra=10^5 in this system should be improved since the thermal conductivity of the base PCM is low. The thermal performance of the PCM may be manipulated by adding the magnesia (MgO) and hybrid Ag/MgO nanoparticles and by using the multilobed capsules. The iterative explicit lattice Boltzmann method (LBM) is implemented to investigate the effects of the nanoparticle loading, aspect ratio (AR) and circumference of the cross-section on the full melting time.

The use of the 2-lobe capsule with the highest AR and increased circumference reduces the full melting time by 37% in contrast to the pure PCM melting in the cylindrical tube. Using the MgO nanoparticles with a lower loading (0.01) within the 2-lobe capsule diminishes the complete melting time for the pure PCM by 55%. It is the best nanofluid-based case when we consider the price of nanoparticles and the capacity of the TES system. The hybrid nanoparticles/PCM composites with (50:50) weight proportions are not prescribed as the increment of the viscosity of the PCM is further than that of the thermal conductivity of the PCM. To decrease the thermal conduction resistance at the bottom section of the horizontal cylindrical capsule, it is suggested to use the multilobed capsule for the pure PCM melting instead of the expensive single nanoparticles

1. Introduction

In the latent heat TES systems, the solar heat could be stored and released by means of the PCMs. Despite the exceptional characteristics of the PCMs such as high storage capacity and chemical stability, the PCMs possess a low thermal conductivity ranging from k=0.15 to 0.3 W.m^{-1}.K^{-1}. This shortcoming abates the heat transfer rate during the charging/discharging cycles.

Hence, the thermal performance of the PCM-based TES systems is unfavorably low. To boost the thermal response of these systems, numerous heat transfer enhancement and optimization techniques have been proposed in the literature accordingly.

1.1. Effect of geometry

The heat transfer characteristics of the TES units are typically related to the size and shape of the PCM-based capsules. Dhaidan and Khodadadi [1] categorized the shapes of containers as spheres, finned shell-and-tube units, cylindrical systems, slender rectangular cavity, and annulus. The inward PCM melting inside horizontal capsules is classified as unconstrained and constrained. In

---

*Corresponding Author: Mahmoud Jourabian, School of Mechanical Engineering, Iran University of Science and Technology, Tehran, Iran
Email: mahmood.jourabian@gmail.com

the constrained melting, the solid PCM is fixed inside the capsule and the densities of solid and liquid phases are almost identical. Also, there is no direct contact melting close to the wall of the capsule.

On the other hand, in the unconstrained melting, the solid phase may be shifted upwardly or downwardly due to the density variation. Ho and Viskanta [2] explored the inward melting within a horizontal cylindrical tube. Ho and Viskanta [2] identified strong secondary recirculating vortices at the bottom section as well as the main natural convection flow. The melting of n-octadecane within an isothermally heated horizontal cylinder was examined by Hirata and Nishida [3]. It was understood that for $Ra<10^5$, the effect of the natural convection on the heat transfer rate from the cylinder was insignificant.

Hirata et al. [4] experimentally researched the melting characteristics of octadecane/ice inside isothermally heated rectangular capsules. The influence of (AR) on the melting was insignificant for $AR<3$. For highly elongated capsules, the melting was faster because the heat transfer area was augmented for the same PCM. Hlimi et al. [5] researched the effects of (Ra) number on the Gallium melting with the natural convection flow inside a horizontal cylinder. It was observed that for $Ra=3\times10^4$, the fluid flow in the melt zone was stable as the viscous force was prevailing.

However, for $Ra=5\times10^6$ and 4×10^7, the Rayleigh-Bénard convection flow was significant in the melt region. Gao et al. [6] explored the two-stage heat transfer characteristics of the constrained paraffin melting within a horizontal cylinder.

In the conduction-dominated regime, the heat transfer characteristics were related to the dimensionless time ($Fo\times Ste$), while in the convection-dominated regime, they were associated with the Fourier, Stefan and Rayleigh numbers. To explore the pure PCM melting inside a 2D cylindrical annulus with the conjugate heat transfer at the inner cylinder, Imani [7] adopted a body-fitted boundary-layer type non-uniform mesh in the LBM. For the higher wall to PCM thermal conductivity ratios ($k_{wall}/k_{pcm}=10,100$), when the thickness of the inner wall was enlarged, it improved the natural convection-dominated melting. Though, for the lower thermal conductivity ratio ($k_{wall}/k_{pcm}=1.0$), the reverse scenario was recorded. The constrained melting of paraffin inside elliptical capsules (prolate and oblate) was studied numerically by Dhaidan [8].

The melting time for the oblate capsule was lesser compared to that for the prolate capsule. The full melting time for the oblate unit was lower than that for the spherical capsule for the similar size, surface area, and heat flux. It was recommended that appropriate orientation and shape of the TES capsule could diminish the negative influence of the low thermal conductivity.

Ho et al. [9] numerically examined the conjugate heat transfer of a PCM inside a circular tube under the external convection cooling. It was concluded that the effects of the conduction within the wall should be considered.

1.2. . Effect of single nanoparticles

Nanotechnology [10-12] is the treatment of nanoparticles to develop energy-efficient thermal systems. The production of nanoparticles is complicated and expensive that necessitates a well-skilled organization. The improvement of the thermal performance of PCMs by means of the conductive mono nanoparticles has been adequately reported in the literature. In fact, the existence of nanoparticles with a higher thermal conductivity with regard to the base PCM could affect the progress of the solid-liquid phase change process significantly. Irwan et al. [13] mentioned that the dispersion of nanoparticles with a certain loading could enhance the thermal performance of PCM-based capsules.

Though, it was stated that the convective effect in the molten PCM was not declined. Sciacovelli et al. [14] simulated the 2D axial-symmetric melting inside a single vertical shell-and-tube latent heat TES unit using the enthalpy method. When the volume fraction of copper nanoparticles was equal to 0.04, the heat flux was boosted by 16%. The existence of copper nanoparticles caused the diminution of the melting time by 15%.

Pahamli et al. [15] researched the melting of paraffin RT50 dispersed with CuO nanoparticles inside a shell-and-tube heat exchanger. It was recorded that nanoparticles augmented the thermal conductivity and dynamic viscosity of the base PCM and they diminished the latent heat of the fusion. When the mass fraction of nanoparticles was augmented from 0.0 to 0.02 and 0.04, the melting time was reduced by 4.56% and 11.16%, respectively.

Yadollahi Farsani et al. [16] scrutinized the melting and solidification of paraffin-alumina nanoparticles composites inside an annular space in a 2D square cavity. When the mass fraction was equal to $\phi=0.02$, the maximum melting rate was achieved. Besides, as the conduction heat transfer was enhanced due to the addition of nanoparticles, it over-compensated the decline of the natural convection effect due to the increment of the viscosity.

Ouikhalfan et al. [17] examined the effects of metal oxide nanoparticles (TiO_2, CuO, Al_2O_3, and ZnO) on the myristic acid (MA) melting. The thermal conductivity of the PCM was enlarged by 1.50, 1.49, 1.45, and 1.37 times, respectively, as the loading of ZnO, Al_2O_3, CuO, and TiO_2 nanopowders was equal to 0.02.

On the other hand, Xiong et al. [18] stated that nanoparticles/PCM composites showed a higher viscosity that degraded the effect of the heat conduction augmentation.

Nizetic et al. [19] stated that the economic aspect of nanotechnology was not adequately discussed since price of materials is also important. Yadav and Sahoo [20] experimentally scrutinized the effects of the natural convection heat transfer on the melting/solidification of stearic acid-Al_2O_3 nanoparticles composites in a concentric cylindrical TES unit. As the mass fraction of

alumina nanoparticles was equal to 0.003, the energy storage rate was escalated by 12.5% compared to the pure PCM.

As could be detected, for each TES system, the efficient thermo-physical properties of composites and optimum volumetric concentration should be proposed. Also, in future studies, the economic aspect of PCM/nanoparticles composites in engineering applications must be evaluated.

1.3. Effect of hybrid nanoparticles

In above papers, only single metallic or non-metallic nanoparticles have been dispersed in PCM-based systems. The metallic nanoparticles possess high thermal conductivities. The PCM/metallic nanoparticles composites are susceptible to the chemical reactions.

On the other hand, the non-metallic nanoparticles could boost the stability, chemical inertness, and they possess lower thermal conductivities. So, it is advantageous to integrate metallic and non-metallic nanoparticles in conventional PCMs. It is the hybrid nanofluids-enhanced PCMs.

Chamkha et al. [21] compared efficiencies of hybrid/single nanoparticles for the octadecane melting within a square cavity with a hot cylinder. It was found that single/hybrid nanofluids showed the Newtonian behavior. The melt front was remarkably deviated when more loadings were prescribed. Once the viscosity parameter was altered, the liquid fraction and phase change interface were not modified considerably.

Ghalambaz et al. [22] researched the melting of ice/hybrid Ag-MgO nanoparticles composites in a square cavity. The PCM melting was accelerated once the effect of the thermal conductivity augmentation exceeded that of the dynamic viscosity enhancement. The temporal variation of the liquid fraction was insignificant when the increment of the dynamic viscosity was higher than the enhancement of the thermal conductivity. Once hybrid Ag (25nm)-MgO (40nm) nanoparticles were added to the base PCM, the melting fraction was increased insignificantly. Also, the hybrid composites demonstrated a faster fusion time in contrast to the water/ MgO nanoparticles composite.

1.4. Motivations

As could be seen, the thermal performance of the constrained inward PCM melting inside an isothermally heated horizontal multilobed capsule with the conjugate heat transfer at the wall has not been evaluated.

The effects of (AR) and circumference of the cross-section of the horizontal tube on the complete melting should be understood. The influences of mono/hybrid nanoparticles on the PCM melting with the natural convection in multilobed horizontal capsules as TES systems should be compared. Finally, the optimum volumetric concentration of nanoparticles (or maximum

TES capacity) with regard to the cost of nanoparticles should be found.

In this article, the constrained inward melting of the ice (Pr=6.2) with Ste=1.0, Ra=10^5 inside isothermally heated multilobed capsules with a conductive wall (made of TiO$_2$) has been studied. The influence of the shape factor of the horizontal capsule on the constrained inward melting of the PCM has been studied. Single MgO and hybrid Ag/MgO nanoparticles are added to the PCM-based capsules in order to boost the solid-liquid phase change process. The existing single-phase enthalpy-based LBM with the double distribution function (DDF) model has been utilized to solve the governing equations of the melting with the natural convection. A quantitative comparison has been established in terms of the time-dependent liquid fraction, average PCM temperature and maximum velocity within the molten PCM.

2. Horizontal multilobed capsules

In this study, the TES systems are isothermally heated horizontal multilobed capsules that are filled with the water/ice as the PCM. They are depicted in figure 1. We compare a horizontal cylinder, 2-lobe and 4-lobe (quatrefoil with more overlap) capsules with the identical cross-sectional area. The conjugate heat transfer at the wall of the tubes has been considered.

$$CS_1 = \pi r_1^2 \tag{1}$$

$$CS_2 = r_2^2 \left(\frac{4\pi}{3} + \frac{\sqrt{3}}{2} \right) \tag{2}$$

$$CS_4 = r_4^2 (2\pi + 4) \tag{3}$$

In the 2-lobe capsule, the distance of two centers of equal-sized lobes is equal to r_2. Quatrefoil capsule is a symmetrical shape that is the outline of four partially-overlapping lobes of the same radius r_4.

In the quatrefoil capsule with more overlap, the distance between centers of the top and bottom lobes (or right and left lobes) is equivalent to $2 \times r_4$. Note that, the initial temperature of the conventional PCM (ice/water) is equal to the melting temperature, so there is no subcooling of the solid PCM in this study.

The outer surface of the conductive wall that is made of Titania (TiO$_2$) is kept at T_l=1.0. The vertical movement of the solid phase toward the bottom of the horizontal capsule is disregarded. For Ra=10^5, there could be the symmetrical melting with the natural convection in the molten PCM. The yellow portion represents the solid phase. In computations, the characteristic length for the cylindrical, 2-lobe, and quatrefoil capsules is defined as $2.0 \times r_1$, $3.0 \times r_2$, and $4.0 \times r_4$, respectively. Thermo-physical properties of the PCMs, Ag, and MgO nanoparticles are provided in table 1. They could be found in [23-24].
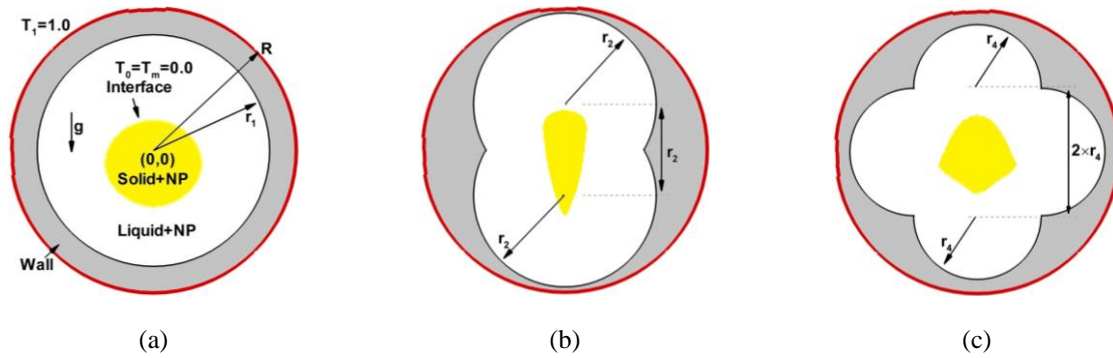
Figure 1. Schematic diagram of the constrained inward melting inside the
horizontal cylindrical (a), 2-lobe(b) and quatrefoil(c) capsules

Table 1. Properties of PCMs and nanoparticles

Property/Material	Ice/water	Paraffin wax	TiO$_2$	Ag	MgO
ρ[kg m^{-3}]	997.1	805	4250	10500	3560
μ [Pa s]	8.9×10^{-4}	6.3×10^{-3}	-	-	-
L [kJ/kg]	335	180	-	-	-
c_p[J kg^{-1} K^{-1}]	4179	2100	686	235	955
k [W m^{-1} K^{-1}]	0.6	0.2	8.95	429	45
β[K^{-1}]	2.1×10^{-4}	1.1×10^{-4}	10.1×10^{-6}	1.89×10^{-5}	9×10^{-6}

3. Governing equations of unsteady melting

(1) Since the volume fraction of nanoparticles (ϕ) is less than 0.02, mono/hybrid nanoparticles/PCM composites show the Newtonian behavior during the phase change process.

(2) The viscous dissipation, compression work and thermal radiation are insignificant. The temperature variation within the PCM-based capsules is finite.

(3) PCM/nanoparticles composites are continuous media. It is assumed that nanoparticles are homogeneously distributed. The PCM and nanoparticles are in the thermodynamic equilibrium condition. From an experimental viewpoint, it is a valid assumption because ultrasonic methods or stabilizers are able to create homogeneous suspensions.

(4) The Boussinesq approximation for the buoyancy term is exploited.

(5) There is no chemical reaction between various components. Nanoparticles are intrinsically inactive and mono/hybrid nanoparticles/PCM composites are considered as stable suspensions. Chamkha et al. [21] emphasized that aforementioned assumptions are acceptable for the mono/hybrid nanoparticles-enhanced PCMs.

(6) There is no difference between densities of two phases.

(7) Hirata and Nishida [3] deduced that the effect of natural convection on the melting heat transfer rate inside an isothermally heated horizontal cylinder was insignificant for $Ra<10^5$.

(8) For $Ra=10^5$, the constrained PCM melting inside horizontal capsules is symmetric and the fluid flow is laminar.

(9) Costa et al. [25] pointed out that the effect of three-dimensionality on the melt fraction and overall Nusselt number was unimportant.

It should be commented that the temporal liquid fraction and average Nusselt number (Nu) on heated surfaces represent the time-dependent evolutions of geometry of the phase change process and heat transfer, respectively.

According to Ref. [26], for a horizontal cylindrical tube with a great length-radius ratio and two adiabatic ends, the heat transfer in the axial direction could be neglected. Ghalambaz et al. [22] provided the following governing equations for the mass, momentum and energy regarding the unsteady constrained PCM melting with the natural convection heat transfer,

$$\frac{\partial \vec{u}_i}{\partial x_i} = 0 \tag{4}$$

$$\frac{\partial \vec{u}_i}{\partial t} + \vec{u}_j \frac{\partial \vec{u}_i}{\partial x_j} =$$
$$\frac{1}{\rho_{nf}}\left(\mu_{eff}\nabla^2\vec{u}_i - \frac{\partial P}{\partial x_i} + (\rho\beta)_{nf}(T - T_{ref})\vec{g}_i\right) \tag{5}$$

$$\frac{\partial T}{\partial t} + \vec{u}_i \frac{\partial T}{\partial x_i} =$$
$$\frac{\partial}{\partial x_i}\left(\frac{k_{nf}}{(\rho c_p)_{nf}}\frac{\partial T}{\partial x_i}\right) - \frac{Z_{nf}}{(\rho c_p)_{nf}}\frac{\partial l_f}{\partial t} \tag{6}$$

The conjugate heat transfer at the wall of horizontal tubes has been considered in this communication. It means that only conduction heat transfer has been solved at the wall by neglecting the last term in the right-hand-side (RHS) of equation (6), whereas the natural convection flow induced in the liquid phase has been considered.

4. Thermo-physical properties of nanofluids

The motivation of the research on hybrid nanofluids is to improve thermal characteristics of TES capsules with respect to thermal conductivity, chemical inertness, material strength and mechanical resistance. Note that the addition of nanoparticles to conventional PCMs diminishes the latent heat of the fusion. Also, the dynamic viscosity of PCM/nanoparticles composites could be higher compared to that of pure PCMs. It may weaken the natural convection heat transfer. Esfe et al. [27] computed the thermal conductivity and dynamic viscosity of Ag-MgO/water hybrid nanofluid. Distilled water was the base fluid and the average diameter of Ag and MgO nanoparticles was equal to 25 nm and 40 nm, respectively. The volumetric concentration of hybrid nanoparticles (with 50% Ag and 50% MgO) was less than 0.02. To eradicate the agglomeration of hybrid nanoparticles in the base fluid, Esfe et al. [27] used an ultrasonic vibrator. Cetyl Trimethyl Ammonium Bromide (CTAB) was applied to acquire the stability and proper dispersion. Zaraki et al. [28] stated that for high loadings of nanoparticles, the non-linear correlations for the thermal conductivity and dynamic viscosity should be developed. Chamkha et al. [21] proposed linear functions for the effective dynamic viscosity and thermal conductivity of hybrid nanofluids as,

$$k_{nf} = (1 + Nc \times \varphi)k_{bf} \tag{7}$$

$$\mu_{nf} = (1 + Nv \times \varphi)\mu_{bf} \tag{8}$$

Nc and Nv are thermal conductivity and dynamic viscosity parameters, respectively. They are functions of size, shape and type of nanoparticles and base fluid, working temperature and preparation technique. The parameters could be straightforwardly obtained by applying linear interpolations on experimental data. Zaraki et al. [28] calculated the density ratio and heat capacity ratio for various nanofluids. It was found that the addition of nanoparticles with the volume fraction of φ=0.03 to the pure fluid changed the density and volumetric heat capacity at the constant pressure less than 3% and 11%, respectively.

Ghalambaz et al. [22] simplified the formulation for the effective thermal diffusivity of the hybrid nanofluids as,

$$\alpha_{nf} = \frac{k_{nf}}{(\rho c_p)_{nf}} = (1 + Nc \times \varphi)\alpha_{bf} \tag{9}$$

Ghalambaz et al. [22] assumed Nc=21 and Nv=6.8 regarding the experiments of Esfe et al. [27]. In this study,

instead of using a simplified formulation for different properties of Ag-MgO/water hybrid nanofluids, we apply the curve-fitting correlations for the thermal conductivity and dynamic viscosity.

Moreover, Nimmagadda and Venkatasubbaiah [29], Ranga Babu et al. [30] and Babar and Ali [31] used the mixture theory to calculate the density, volumetric heat capacity at constant pressure and buoyancy coefficient for single/hybrid nanofluids as,

$$k_{nf} =$$

$$\left(\frac{0.1747 \times 10^5 + \varphi}{0.1747 \times 10^5 - a \times \varphi + b \times \varphi^2 + c \times \varphi^3}\right)k_{bf}$$

$$\tag{10}$$

$$a = 0.1498 \times 10^6,$$

$$b = 0.1117 \times 10^7,$$

$$c = 0.1997 \times 10^8$$

$$\mu_{nf} = (1 + 32.795 \times \varphi - 7214 \times \varphi^2 + 714600 \times \varphi^3 - 0.1941 \times \varphi^4 \times 10^8)\mu_{bf} \tag{11}$$

$$\rho_{nf} = \varphi_1 \times \rho_{np1} + \varphi_2 \times \rho_{np2} + (1 - \varphi_1 - \varphi_2)\rho_{bf}, \tag{12}$$

$$\varphi = \varphi_1 + \varphi_2$$

$$(\rho c_p)_{nf} = \varphi_1 \times (\rho c_p)_{np1} + \varphi_2 \times (\rho c_p)_{np2} + (1 - \varphi)(\rho c_p)_{bf} \tag{13}$$

$$(\rho\beta)_{nf} = \varphi_1 \times (\rho\beta)_{np1} + \varphi_2 \times (\rho\beta)_{np2} + (1 - \varphi)(\rho\beta)_{bf} \tag{14}$$

The micro-convection model developed by Patel et al. [32] and the Brinkman model have been applied in this study to calculate the thermo-physical properties of single nanofluids. The value of c' is 3.6×10^4. Moreover, the diameter of MgO nanoparticles is 40.0 nm at 300K. The molecular size of the base fluid is equal to 2.0 Å.

$$k_{nf} = k_{bf} + k_{np}\frac{A_{np}}{A_{bf}} + c'k_{np}Pe\frac{A_{np}}{A_{bf}} \tag{15}$$

$$\mu_{nf} = \frac{\mu_{bf}}{(1 - \varphi)^{2.5}} \tag{16}$$

$$\frac{A_{np}}{A_{bf}} = \frac{d_{np}}{d_{bf}} \times \frac{\varphi}{(1 - \varphi)} \tag{17}$$

$$Pe = \frac{|\vec{u}_p|d_{np}}{\alpha_{bf}} \tag{18}$$

$$|\vec{u}_p| = \frac{2k_bT}{\pi\mu_{bf}d_{np}^2} \tag{19}$$

5. Single-phase enthalpy-based LBM

Costa et al. [25] mentioned that the instantaneous liquid fraction in experiments could be underestimated. Also, valleys of the melt front at the bottom of the horizontal cylinder were not detected in experiments. Costa et al. [25] stated that in order to acquire an in-depth study on the PCM melting, the computational time should be decreased. In recent years, the LBM has been developed based on the kinetic theory and lattice gas automata. The LBM is a mesoscopic technique that resolves the Boltzmann equation using the Bhatnagar-Gross-Krook (BGK) approximation. In contrast to conventional CFD techniques, the LBM gives some advantages, for instance, the straightforward calculation, parallel programming and the absence of a pressure Poisson equation. The fluid flow is manifested by a lattice. The specific particle distribution functions (PDFs) are defined to calculate thermo-physical properties. The PDFs are collections of particles with a specific direction that displace with a specific velocity. They are calculated and updated spatially. The LBM consists of two stages called the collision and streaming. In the first stage, the arriving particles in terms of PDFs interact and exchange the momentum. In the second stage, PDFs are shifted in the lattice directions from one lattice to the adjacent lattice.

The discretized Boltzmann equations for velocity and temperature fields are developed as,

$$f_i(x + \vec{c}_i \Delta t, t + \Delta t) - f_i(x,t) = -\frac{\left(f_i(x,t) - f_i^{eq}(x,t)\right)}{\tau_I} + \Delta t \times \vec{F}_i \tag{20}$$

$$g_i(x + \vec{c}_i \Delta t, t + \Delta t) - g_i(x,t) = -\frac{g_i(x,t) - g_i^{eq}(x,t)}{\tau_{II}} + \Delta t \vec{Q}_i \tag{21}$$

The source terms in this study are calculated as,

$$\vec{F}_i = -3\rho_{lbm}\omega_i(g\beta)_{lbm}(T - T_{ref})\vec{c}_i \tag{22}$$

$$\vec{Q}_i = -\frac{\omega_i}{Ste}\left[\frac{l_f(t + \Delta t) - l_f(t)}{\Delta t}\right] \tag{23}$$

The DDF model with the D2Q9 lattice directions is applied, similar to Ramazani Sarbandi et al. [33] and Yazdi et al. [34],

$$\vec{c}_i = \begin{cases} (0,0) & i = 0 \\ (cos[A], sin[A]) \times c & i = 1,2,3,4 \\ \sqrt{2}(cos[B], sin[B]) \times c & i = 5,6,7,8 \end{cases} \tag{24}$$

$$A = (i - 1) \times (\pi/2), \; B = (2(i-5)+1) \times (\pi/4)$$

$$c = \frac{\Delta x}{\Delta t} = 1.0 \tag{25}$$

$$\omega_i = \begin{cases} 4/9 & i = 0 \\ 1/9 & i = 1,2,3,4 \\ 1/36 & i = 5,6,7,8 \end{cases} \tag{26}$$

The equilibrium distribution functions (EDFs) for velocity and temperature fields and pertinent variables in the LBM are computed as Himrane et al. [35],

$$f_i^{eq}(x,t) =$$

$$\omega_i\rho_{lbm}\begin{bmatrix} 1 + 3 \times (\vec{c}_i.\vec{u}_{lbm}) + 4.5 \times (\vec{c}_i.\vec{u}_{lbm})^2 \\ -1.5 \times (\vec{u}_{lbm}.\vec{u}_{lbm}) \end{bmatrix} \tag{27}$$

$$\rho_{lbm} = \sum_i f_i(x,t) \tag{28}$$

$$\rho_{lbm}\vec{u}_{lbm} = \sum_i \vec{c}_i f_i(x,t) \tag{29}$$

$$P_{lbm} = \rho_{lbm}/3 \tag{30}$$

$$T = \sum_i g_i(x,t) \tag{31}$$

$$l_f(t) = \begin{cases} 0 & T \le 0 \\ \dfrac{T - T_0}{T_1 - T_0} & 0 < T < T_1 \\ 1 & T \ge 1 \end{cases} \tag{32}$$

$$Ra = \frac{g\beta(T_1 - T_0)l^3}{\nu_{bf}\alpha_{bf}},$$
$$Ste = \frac{(c_p)_{bf}(T_1-T_0)}{z_{bf}}, \qquad Pr = \frac{\nu_{bf}}{\alpha_{bf}} \tag{33}$$

$$Pr_{nf} = \frac{\mu_{nf}}{\rho_{nf}\alpha_{nf}},$$

$$\nu_{nf(lbm)} = \nu_{bf(lbm)} \times \left(\frac{\mu_{nf}}{\rho_{nf}} \times \frac{\rho_{bf}}{\mu_{bf}}\right), \tag{34}$$

$$\nu_{bf(lbm)} = \frac{3}{10}, \; \alpha_{nf(lbm)} = \frac{\nu_{nf(lbm)}}{Pr_{nf}},$$

$$\nu_{nf(lbm)} = (\tau_I - 0.5)c_s^2\Delta t, c_s = \frac{\sqrt{3}}{3}, \tag{35}$$

$$\alpha_{nf(lbm)} = (\tau_{II} - 0.5)c_s^2\Delta t \tag{36}$$

6. Validation of LBM code

Khanafer et al. [36] researched the buoyancy-driven heat transfer enhancement of copper/water nanofluid in a 2D enclosure for various Grashof numbers and volume fractions.

The AR of the cavity was equal to 1.0 and the diameter of copper nanoparticles was equal to 10 nm. The left vertical wall was isothermally heated (T_1) while the right vertical wall was isothermally cooled (T_0). The top and bottom walls were adiabatic.

(a)   (b)
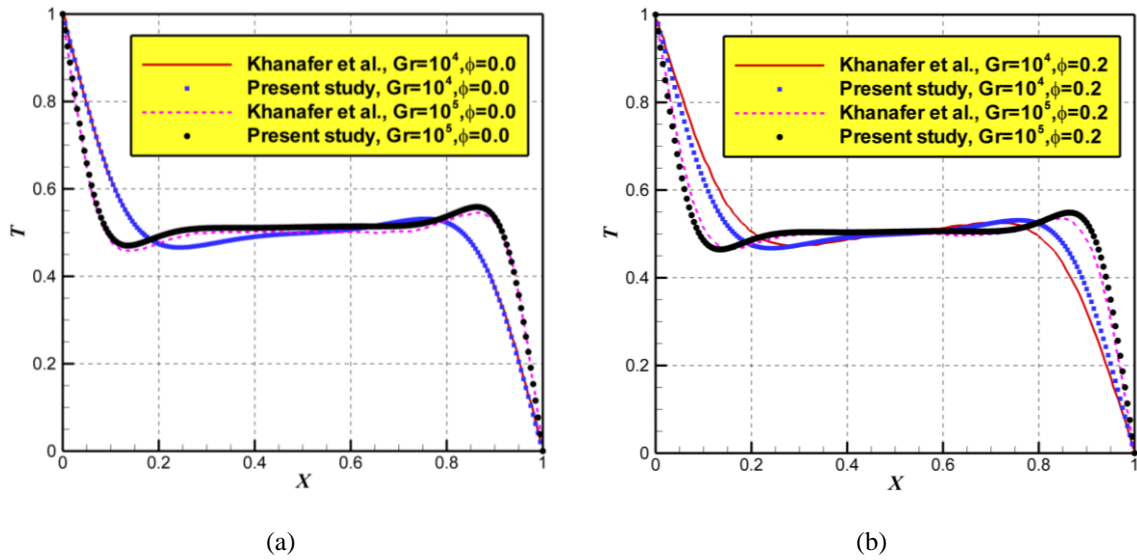
Figure 2. Validation (I): temperature of the pure water (a) and Cu/water nanofluid with ϕ=0.2 (b) along the mid-plane of the square cavity against Khanafer et al. [36]

The addition of nanoparticles to the base water (Pr=6.2) significantly raised the heat transfer rate for each Grashof number. The heat transfer rate was elevated as the loading of nanoparticles was increased. The existence of nanoparticles in the base water changed the structure of the fluid flow.

In figure 2, temperature variations on the axial midline for Gr=10^4-10^5 and ϕ=0.0, 0.2 are compared against Khanafer et al. [36]. The grid size of 200×200 is selected. The kinematic viscosity of the pure water in the LBM code is equivalent to 0.3. For ϕ=0.2 and Gr=10^4, the maximum error for the temperature is equivalent to 7%.

In figures 3 and 4, the streamlines and isotherms for ϕ=0.2, Pr=6.2, Gr=10^4 are compared. As could be detected, a satisfactory agreement has been achieved.

(a)   (b)
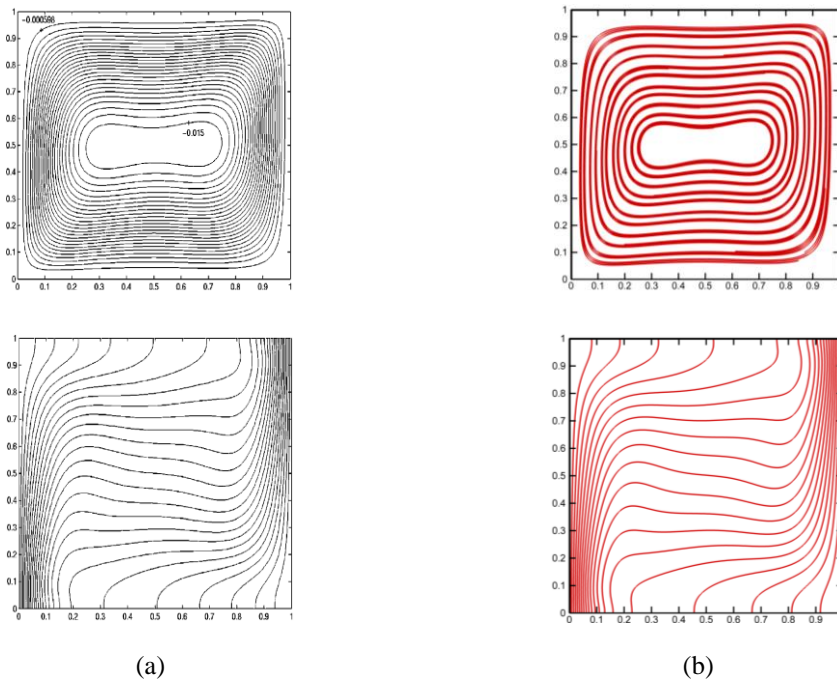
Figure 3. Validation (I): comparisons in terms of the streamlines (top) and isotherms (bottom) for the pure water for Pr=6.2, Gr=10^4 between Khanafer et al. [36] (a) and present study (b)
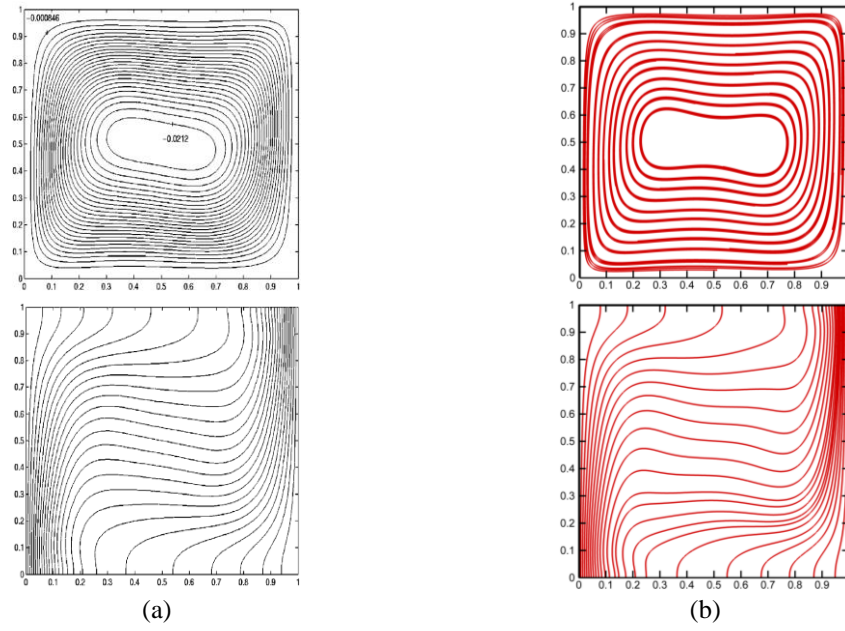
Figure 4. Validation (I): comparisons in terms of the streamlines (top) and isotherms (bottom) for the copper/water nanofluid with ϕ=0.2 at Pr=6.2, Gr=10^4 between Khanafer et al. [36] (a) and present study (b).
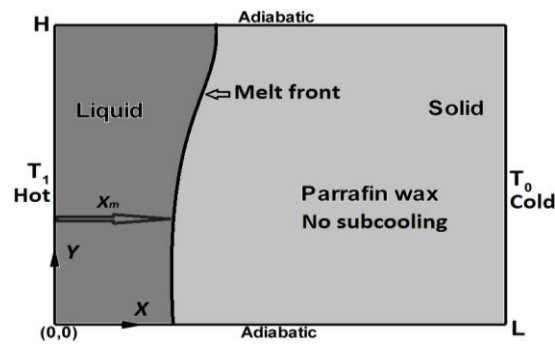
Figure 5. Schematic of the pure paraffin wax melting in a rectangular cavity
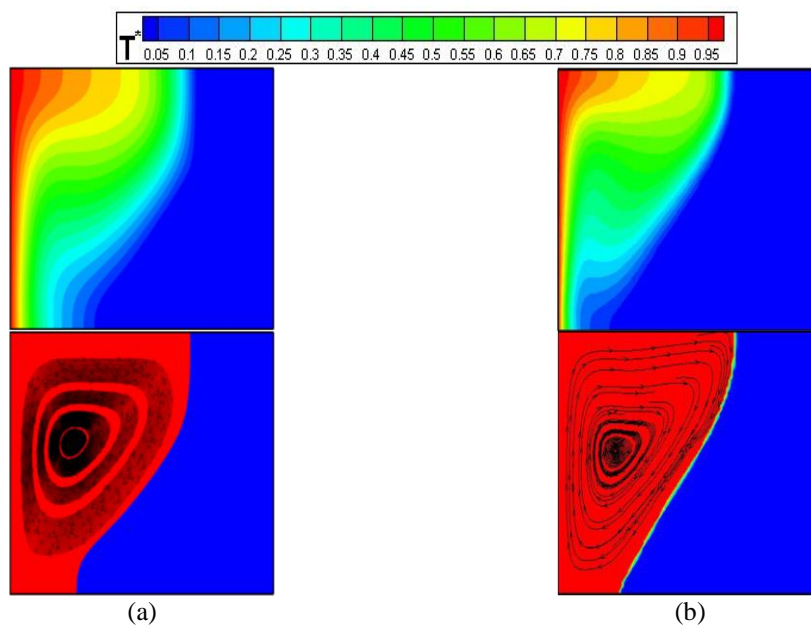
Figure 6. Validation (II): the temporal phase field, temperature field and flow field for the pure paraffin wax melting in a rectangular cavity (a) with regard to Chen et al. [37] (b)

In figure 5, the pure paraffin wax melting in a rectangular capsule has been considered as the second validation case. The key dimensionless numbers are equal to $Ra=10^5$, $Pr=5.0$ and $Ste=1.0$.

The lattice grid size of 100×65 has been used. In figure 6, phase, temperature and flow fields at the dimensionless time of θ=0.2 are shown. A well agreement with regard to the study of Chen et al. [37] has been obtained.

Also, there is a qualitative agreement between the present study and the experiments of Chen et al. [37] in terms of the shape of the solid-liquid interface.

The height-averaged location of the solid-liquid interface could be estimated by,

$$S_{av}(t) = \frac{1}{H}\int_0^H x_m dy \propto HRa^{1/4}\theta \qquad (37)$$

It could be seen in figure 7 that the present LBM code could simulate satisfactorily the PCM melting with the natural convection heat transfer in TES capsules.

7. Grid independence of solution

The existing 2D LBM code has been used on a laptop with the Dual cores CPU and 4G RAM. As the pure ice is fully melted inside the horizontal capsule, the code stops running.

To check and evaluate the grid independence of the solution, the pure PCM melting inside a horizontal cylindrical tube with the conductive wall (made of TiO2) is examined. The important dimensionless numbers are equivalent to Pr=6.2, Ste=1.0 and Ra=105. In figure 8, the mesh independence tests are shown.

As the grid size is increased from 14400 to 25600, the full melting time is boosted by 16.66%. As the grid size is

augmented from 25600 to 40000, full melting time is enlarged by 14.28%. And finally, when the grid size is increased from 40000 to 57600, the full melting time is escalated by 10.41%. It is revealed that an equally spaced grid of 200×200 could be sufficient to simulate the solid-liquid phase change process. An extra increase of the mesh size causes a lesser variation of the complete melting time.

It should be said that the Mach number is $Ma=0.19$ and the incompressibility condition is satisfied based on the following criterion,

$$\nu = 0.3 = \sqrt{\frac{Ma^2 M^2 Pr\, c^2}{Ra}} \qquad (38)$$

M is the number of lattices in the vertical direction, parallel to the gravitational force. It must be commented that the complete melting time is equal to 231.45 seconds for the mesh size of 200×200. As Jourabian et al. [38] mentioned, the characteristic velocity defined for the natural convection flow should be smaller than the speed of the sound. In this study, the characteristic velocity is equal to,

$$\left|\vec{V}\right| = \sqrt{(g\beta)_{lbm} \times l \times \Delta T} = 0.4 \times c_s \qquad (39)$$

8. Results

8.1. Pure PCM melting

In figure 9, we show time-dependent variations of isotherms (right-hand-side) and streamlines (left-hand-side) for the pure ice melting in the horizontal cylinder, 2-lobe and quatrefoil capsules with the conductive wall.
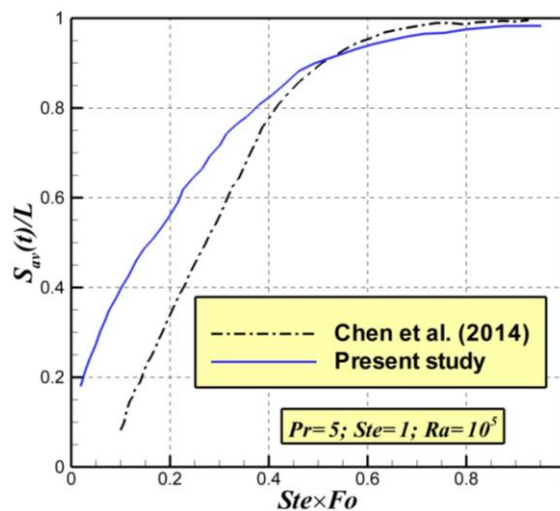
Figure 7. Validation (II): the instantaneous average melting front position for the pure paraffin

wax melting in a rectangular cavity in contrast to Chen et al. [37]
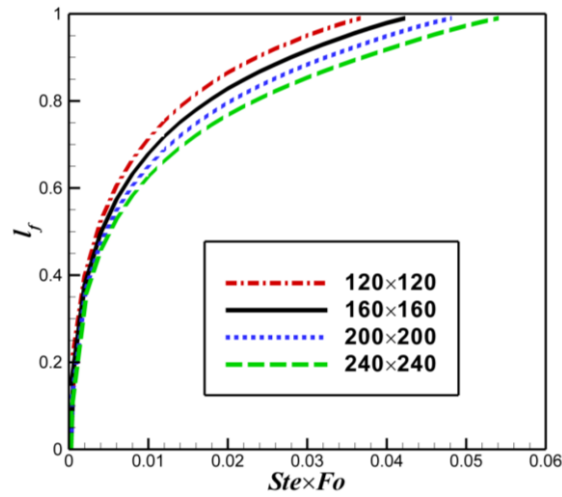
Figure 8. Lattice mesh tests for the pure PCM melting inside horizontal
cylindrical capsule with the conductive wall

(a)

$\theta=1.8\times10^{-4}$ $\theta=1.19\times10^{-2}$ $\theta=3.59\times10^{-2}$

(b)

$\theta=1.8\times10^{-4}$ $\theta=1.19\times10^{-2}$ $\theta=2.9\times10^{-2}$

(c)

$\theta=1.8\times10^{-4}$ $\theta=1.19\times10^{-2}$ $\theta=3.39\times10^{-2}$
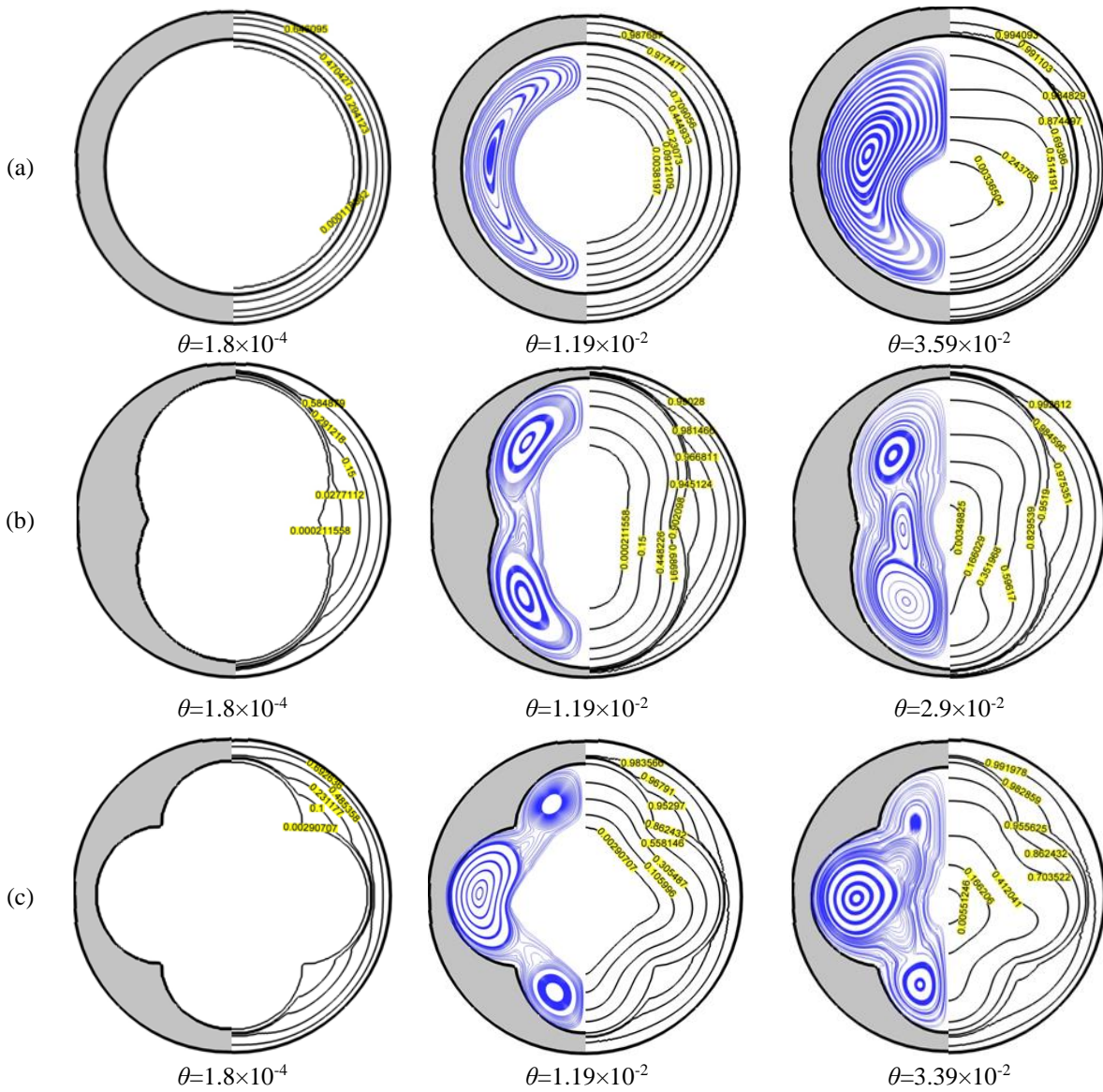
Figure 9. Time-dependent isotherms and streamlines for the pure PCM melting in the
horizontal cylindrical tube and multilobed capsules.

The thermal energy is transferred by the conductive wall to the solid PCM by the conduction heat transfer. Regarding the cylindrical capsule, in the initial moments of the melting process ($\theta \leq 2.0 \times 10^{-4}$), the solid-liquid interface resembles the inner wall of the conductive shell. It demonstrates the domination of the conduction inside the thin liquid layer between the solid phase and inner wall. Also, there is no recirculating vortex inside the melt zone. As the time elapses more, the thermal energy is further transferred to the solid PCM and the melt zone is enlarged. One recirculating vortex in the clock-wise direction is formed within the melt zone regarding the half of the TES capsule. Also, the natural convection flow starts to be developed. In fact, the liquid phase is warmed up adjacent to the inner surface of the conductive wall and it is moved vertically toward the top section of the horizontal capsule. After that, it is cooled down along the solid-liquid interface. At $\theta = 3.5 \times 10^{-2}$, the center of recirculating vortex is shifted upwardly with the respect to the horizontal mid-plane. It is due to intensifying effect of the natural convection in the top section of the horizontal cylinder. The initial concentric shape of the solid-liquid interface is totally deformed. The melting front resembles to an oblate. This is in accordance with the study of Rieger and Beer [39]. It was reported that for $Ste > 0.1$, the shape of the solid phase was oblate in final moments of the confined ice melting. Hirata and Nishida [3] found that the effect of the natural convection on the PCM melting within an isothermally heated horizontal cylinder was not insignificant for $Ra \geq 10^5$.

On the other hand, for the paraffin RT50 melting, Chen et al. [40] concluded that in comparison with the horizontal circular capsule, the use of the oblate ellipse decreased the charging time by 10.2%. It was attributed to 5.2% augmentation of the circumference that characterizes the heat transfer area. The melting time of the PCM in the vertically elongated capsule was longer than that in the cylinder. For cylindrical TES units, it was recorded that the larger the thickness of the PCM along the gravitational direction was, the longer the time was required for the unconstrained melting. A large thickness of the PCM along the gravity reduced the strength of the natural convection. For the close-contact melting of the PCM within a horizontal elliptical tube, Chen et al. [41] understood that when the ratio between long vertical radius and short horizontal radius was higher than 1.0, the melting rate was escalated compared to the cylindrical tube. Also, the melting rate in the prolate tube was higher than that in the oblate one. As a result, the driving force (gravity) along the long radius should be applied to enhance the PCM melting.

Fomin and Wilchinsky [42] communicated that the rate of the melting was higher for the elongated capsules in comparison with the oblate ones.

It was due to the smaller thickness of the molten layer and the higher pressure from the solid phase. For oblate capsules, however, the pressure was distributed uniformly on the solid phase. So, a quick decrease of the PCM

melting time in the elongated capsules was reported compared to the oblate ones.

In this study, in order to minimize the thermal conduction resistance within the wall, we have used a more conductive material like copper other than TiO2 for the wall. Besides, according to Imani [7], we could diminish the thickness of the conductive wall at the bottom to expedite the PCM melting. Because the improvement of the ratio between thermal conductivities of the wall and PCM (=14.91) is not the scope of the current study, the melting of the pure PCM should be enhanced in terms of AR and circumference of the cross-section.

(a)

(b)

(c)
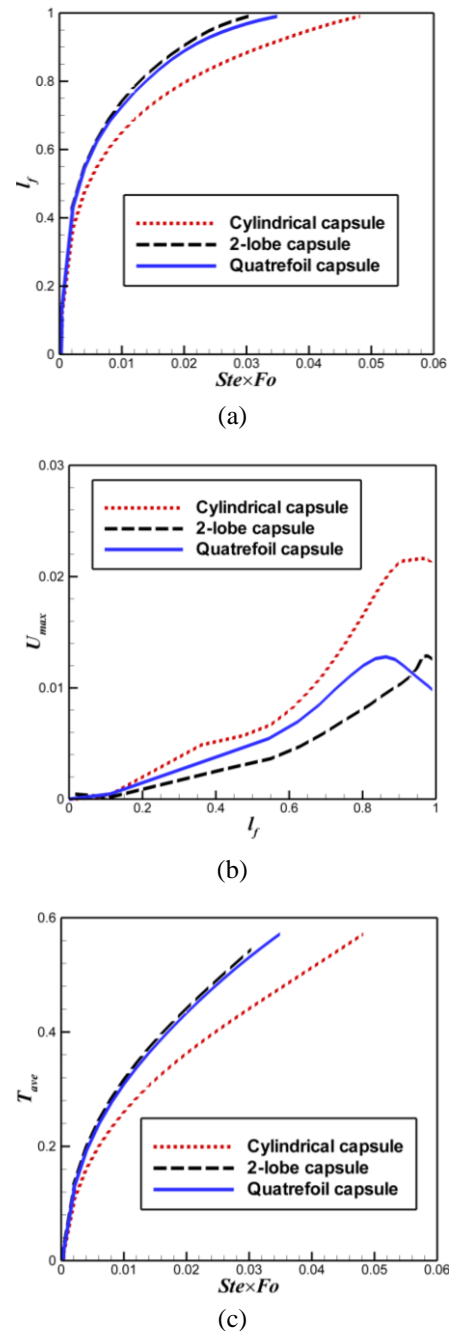
Figure 10. Temporal evolutions of the liquid fraction, maximum velocity and average PCM temperature for the pure PCM melting inside horizontal capsules

For the same cross-section area (identical TES capacity), the circumference and AR of the horizontal tube and multilobed capsules are computed as,

$$cf_1 = 2 \times \pi \times r_1, AR_1 = 1.0 \qquad (40)$$

$$cf_2 = \frac{8\pi}{3} \times r_2 = 1.05 \times cf_1, AR_2 = 1.5 \qquad (41)$$

$$cf_4 = 4 \times \pi \times r_4 = 1.1 \times cf_1, AR_4 = 1.0 \qquad (42)$$

It is noticed that a lesser portion of the solid phase remains once the 2-lobe capsule is used. With this capsule, there is highest AR with the increased circumference of the cross-section in contrast to the cylindrical tube.

In the 2-lobe capsule, the thickness of the conductive wall at the bottom is smallest compared to other capsules. It results in the acceleration of the pure PC melting with the natural convection.

In figure 10a, we display temporal evolutions of the liquid fraction for the pure PCM melting inside cylindrical and multilobed capsules with the conjugate heat transfer at the wall. When 2-lobe and quatrefoil capsules are used, the complete melting time is diminished by 37% and 27%, respectively, with respect to the cylindrical capsule.

To estimate the influence of the curvature on the intensity of the natural convection, temporal evolutions of the maximum velocity versus the liquid fraction are depicted in figure 10b. At the onset of the phase change process, the fluid flow is weak and the thickness of the molten PCM is small. As the process progresses more, the thickness of the molten PCM augments and the natural convection is intensified. Subsequently, the maximum velocity gets an apex.

Finally, the graph of the maximum velocity for the 4-lobe capsule is decreased that represents the attenuation of the natural convection.

$\theta=1.9\times10^{-3}$ $\theta =1.79\times10^{-2}$ $\theta=3.19\times10^{-2}$

$\theta=1.9\times10^{-3}$ $\theta=9.9\times10^{-3}$ $\theta=1.99\times10^{-2}$

$\theta=1.9\times10^{-3}$ $\theta=1.39\times10^{-2}$ $\theta=2.59\times10^{-2}$
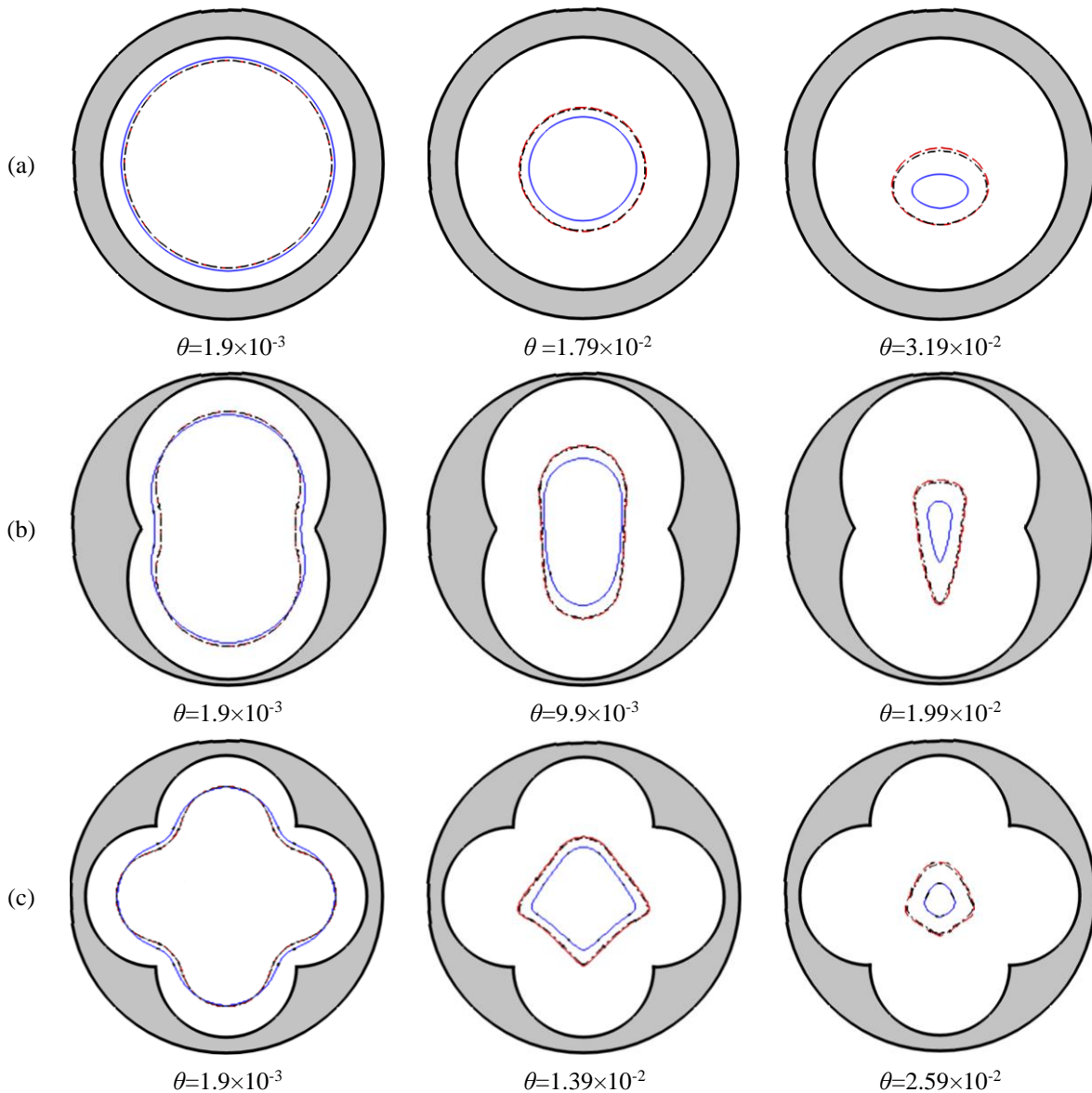
Figure 11. Solid-liquid interface for the pure PCM (long dashed line), mono nanoparticles/PCM composite with the volume fraction of 0.01 (solid line) and hybrid nanoparticles/PCM composite with the volume fraction of 0.01 (dashed dot line) inside the cylindrical tube (a), 2-lobe capsule (b) and 4-lobe capsule (c)

It is observed that the application of multilobed capsules abates the magnitude of the maximum velocity in contrast to the cylindrical tube. The natural convection flow is mostly dwindled in the 2-lobe capsule with the highest AR.

In figure 10c, we observe that the use of multilobed capsules amplifies the PCM average temperature (Tave). In comparison with the cylindrical tube, it takes a lesser time to reach a critical temperature for the pure PCM by means of multilobed capsules. It is due to the augmentation of the circumference. However, the increase of the number of lobes from 2.0 to 4.0 does not affect the average PCM temperature considerably. Finally, for the pure PCM melting, the best thermal performance could be acquired as the AR of the cross-section is highest and the circumference is elevated.

8.2. NEPCM melting

In figure 9, we show time-dependent variations of isotherms (right-hand-side) and streamlines (left-hand-side) for the pure ice melting in the horizontal cylinder, 2-lobe and quatrefoil capsules with the conductive wall

Xie et al. [43] confirmed that amid MgO, TiO2, ZnO, Al2O3 and SiO2 nanoparticles, MgO-ethylene glycol (EG) nanofluid had superior features such as the maximum thermal conductivity and minimum viscosity. Xie et al. [43] measured the viscosity and it was verified that MgO-EG nanofluids showed a Newtonian rheological behavior. Mahmoodi [44] investigated effects of the Rayleigh number, volumetric concentration of nanoparticles and various types of water-based nanofluids on the free convection and heat transfer in an enclosure with a thin heater. Mahmoodi [44] found that for Ra=105-106, compared to Cu/water and TiO2/water nanofluids, Ag/water nanofluid was more effective to boost the heat transfer rate. For the solid-liquid mixtures, Xie et al. [43] commented that enhancements of the thermal conductivity and viscosity due to nanopowders were much higher than values obtained by means of classical models. Xie et al. [43] emphasized that these models only considered the volumetric concentration and overlooked the diameter. Corcione [45] adopted two empirical correlations with 1.86% error for the evaluation of the thermal conductivity and dynamic viscosity of nanofluids. The diameter of nanoparticles and the temperature were included from experiments.

In this study, it is understood that there is no difference between the empirical formulation and the Brinkman model regarding the calculation of the dynamic viscosity of single MgO/water nanofluid with ϕ=0.01. Furthermore, the US Research Nanomaterials Inc. provides that the price per 1.0 gram of Ag nanoparticles with the diameter of 20.0 nm, and 1.0 gram of MgO nanoparticles with the diameter of 40.0 nm could be $25 and $1.56, respectively. Hence, the cost of hybrid nanoparticles with 50:50 weight proportions is 8.5 times more than that of MgO nanoparticles in each loading. Regardless of the type of

nanofluids, with the increment of the volume fraction, the storage capacity of the TES system is degraded and the cost is increased proportionally.

In figure 11, instantaneous evolutions of solid-liquid interfaces for the pure PCM melting (long dashed line), single nanoparticles/PCM composites with ϕ=0.01 (solid line) and hybrid nanoparticles/PCM composites with ϕ=0.01 (dashed dot line) are given. The addition of single MgO nanoparticles with ϕ=0.01, dnp=40nm diameter at T=300K enhances the thermal conductivity of the base PCM from 0.6 to 2.62. It also increases the dynamic viscosity by 2.47%. Consistent with Xie et al. (2010), MgO nanoparticles facilitate the transfer of the thermal energy from the conductive wall to the solid phase in all capsules. It results in the progress of the melt zone and the acceleration of the process. On the other hand, the dispersion of hybrid Ag/MgO nanoparticles with ϕ=0.01 enhances the thermal conductivity by 8.3% and it increases the dynamic viscosity of the base PCM by 12.7%. It is observed that the addition of hybrid nanoparticles does not enlarge the melting rate in contrast to the pure PCM melting because the increment of the viscosity is more than the augmentation of the thermal conductivity. Although single MgO and Ag nanoparticles could boost the heat transfer characteristics of the constrained inward PCM melting, the PCM/hybrid nanoparticles composite with 50:50 weight proportions is not recommended based on the price-performance analysis.

In figure 12, we depict the influences of the volume fraction of single/hybrid nanoparticles on the temporal evolutions of the liquid fraction, maximum velocity within the liquid phase and average PCM temperature. It must be pointed out that the increase in the volume fraction of MgO nanoparticles from 0.01 to 0.02 improves the thermal conductivity and dynamic viscosity by 79% and 2.63%, correspondingly. Similarly, as the loading of hybrid Ag/MgO nanoparticles is augmented from 0.01 to 0.02, the thermal conductivity and dynamic viscosity are boosted by 6.92% and 22.53%, respectively.

In table 2, we illustrate reductions in the full melting time of the pure PCM in each horizontal capsule once single/hybrid nanoparticles are incorporated

In comparison with the pure PCM melting, the addition of single MgO nanoparticles in all capsules intensifies the maximum velocity and natural convection flow within the molten PCM. The more the loading of single magnesia nanoparticles is augmented, the more the effect of the convection is strengthened. It could be deduced from the improvement in the maximum velocity. It should be commented that a lower loading of MgO nanoparticles is more effective to diminish the full melting time compared to the higher loading (0.02). It is due to the negative effect of the increased viscosity. This is in accordance with the study of Bayat et al. [46] who evaluated the performance of a heat sink filled with paraffin and different percentages of alumina and copper oxide nanoparticles. Bayat et al. (2018) reported that the increase in the volume fraction from ϕ=0.04 to 0.06 did not change the liquid fraction. It

was due to the adverse effect of greater levels of nanoparticles

The lessening of the full melting time in each capsule due to the hybrid Ag-MgO nanoparticles is detected. Though, the rate of the decrease by means of the hybrid Ag-MgO nanoparticles is significantly lower compared to single MgO nanoparticles since the thermal conductivity of the base PCM due to hybrid nanoparticles is improved lesser. With the increase of the volume fraction of the hybrid nanoparticles from ϕ=0.01 to 0.02, the maximum velocity and melt fraction are improved infinitesimally. It is due to the augmentation of the dynamic viscosity that degrades the natural convection effect.

Bayat et al. [46] reported that with the volume fraction of ϕ=0.02, 0.04 of non-metallic nanoparticles, the effect of the increased thermal conductivity surpassed the effect of the augmented viscosity, and thus, the heat sink temperature was abated. Analogously, in our study, the

required time to reach the critical temperature for the PCM is increased when the volumetric concentration of MgO nanoparticles is amplified from 0.01 to 0.02.

In table 3, we compare efficiencies of using single/hybrid nanoparticles and multilobed configurations to abate the complete melting time with regard to the pure PCM melting in the horizontal tube. Accordingly, the maximum reduction of the full melting time is by 55% by means of single MgO nanoparticles with ϕ=0.01 in the 2-lobe capsule. Moreover, the thermal storage capacity is highest and the cost is least with this effective composite.

In our study, we do not implement a more conductive material for the wall. The thermal conduction resistance at the bottom of the capsule has been minimized because the thickness of the wall is reduced (as the highest AR with the increased circumference is applied) and the thermal conductivity of the base PCM is augmented due to single non-metallic nanoparticles.
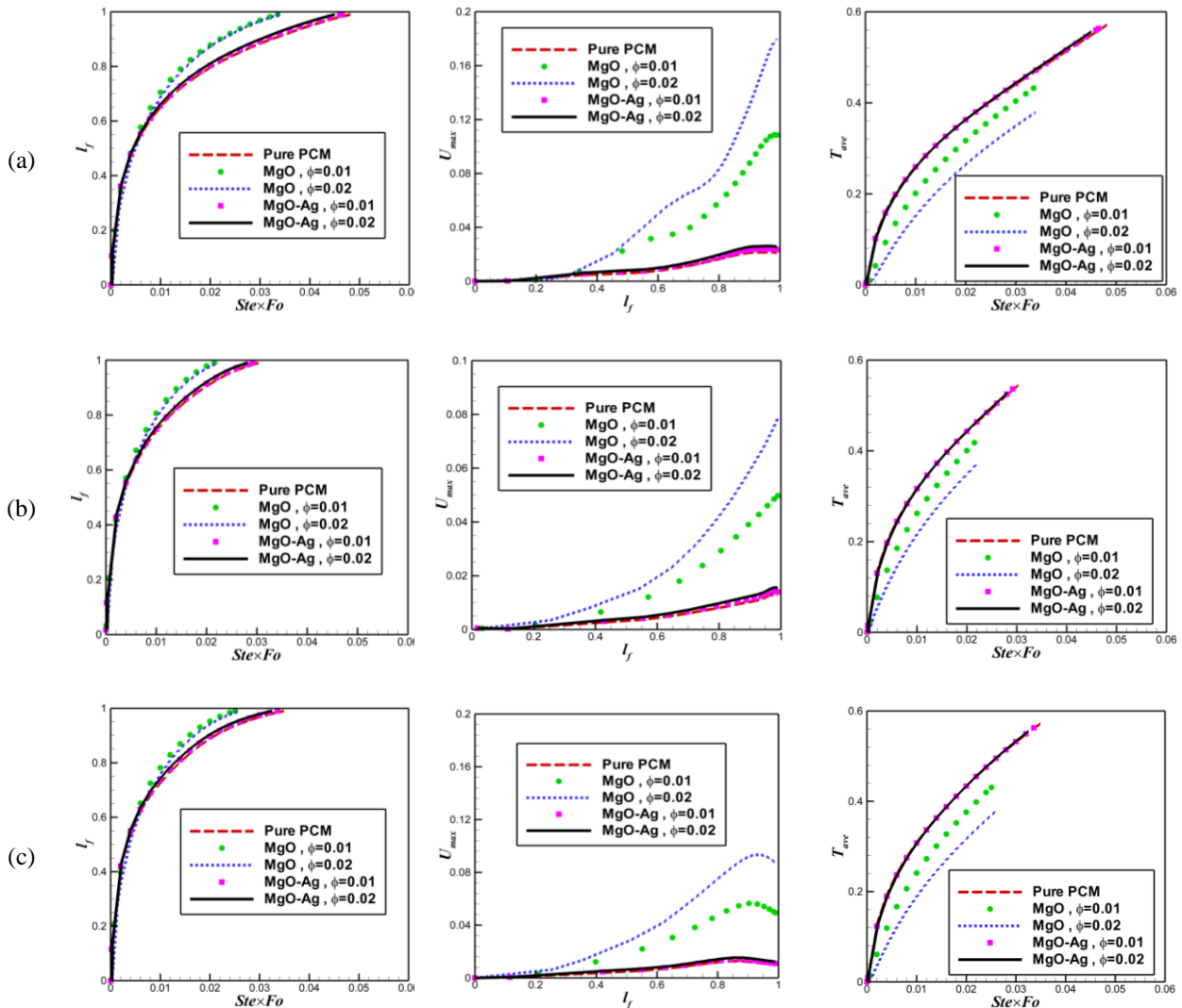
Figure 12. Time-wise variations of the liquid fraction, maximum velocity inside the molten PCM and average PCM temperature for the nanoparticles/PCM composites within the cylindrical tube (a), 2-lobe capsule (b) ad quatrefoil capsule (c)

Table 2. The variation of the full melting time due to nanoparticles compared to the pure PCM melting in each capsule

MgO			
	Cylinder	2-lobe capsule	Quatrefoil capsule
ϕ=0.01	-30.35%	-29.04%	-28.36%
ϕ =0.02	-29.52%	-26.4%	-25.5%
Hybrid Ag/MgO			
	Cylinder	2-lobe capsule	Quatrefoil capsule
ϕ=0.01	-3.5%	-3.96%	-3.72%
ϕ =0.02	-6.44%	-7.26%	-6.87%

Table 3. The variation of the complete melting time caused by nanoparticles in contrast to the pure PCM melting inside the horizontal cylindrical tube

MgO		
	2-lobe capsule	Quatrefoil capsule
ϕ=0.01	-55%	-47.87%
ϕ =0.02	-53.63%	-45.94%
Hybrid Ag/MgO		
	2-lobe capsule	Quatrefoil capsule
ϕ=0.01	-39.5%	-30.14%
ϕ =0.02	-41.58%	-32.43%

At the end, it is essential to notice that the complete melting time for the single nanoparticles/PCM composite with ϕ=0.01 inside the cylindrical capsule is identical to that for the pure PCM melting in the 2-lobe capsule. It confirms that the addition of expensive nanopowders is not always practical to enhance the heat transfer characteristics of the conventional PCMs in TES units.

Conclusion

In this communication, in order to accelerate the constrained inward melting inside isothermally heated horizontal cylinder, we modified the AR and circumference of the cross-section and the thermal conductivity of the base PCM. For the pure paraffin wax melting in the rectangular enclosure, the qualitative agreement between the present LBM study and experiments in terms of the shape of the solid-liquid interface was obtained. For the hybrid nanoparticles/PCM composites, the curve-fitting correlations for the thermal conductivity and dynamic viscosity were implemented. For the single nanoparticles/PCM composites, however, the micro-convection model was presumed.

(1) The thermal conduction resistance at the bottom of the 2-lobe capsule was lowest compared to other isothermally heated horizontal capsules. For the pure PCM melting, the best thermal performance was obtained by means of the 2-lobe capsule because the *AR* of the cross-section was highest and its circumference was elevated in contrast to the horizontal cylindrical tube. It required a lesser time to attain a critical temperature of the pure PCM with multilobed capsules since the circumference was enhanced.

(2) The minimum full melt time was realized with the use of single MgO nanoparticles (ϕ=0.01) inside the 2-lobe capsule. The TES capacity was highest and the cost was least by means of this effective composite. The thermal conduction resistance at the bottom was minimized as the highest AR with the increased circumference of the cross-section was applied and the thermal conductivity of the base PCM was augmented.

(3) In each horizontal capsule, the reduction of the full melting time due to the existence of hybrid Ag-MgO nanopowders was also detected. Nevertheless, the rate of the decrease was considerably lower compared to the single MgO nanoparticles.

(4) It was understood that the augmentation of the volume fraction more than 0.01 was not effective to advance the thermal characteristics of the isothermally heated horizontal PCM-based capsules.

(5) It was recommended to modify the curvature of the cross-section of horizontal PCM-based capsules to lessen the charging time. The addition of expensive nanopowders was not always practical to boost the thermal performance of conventional PCMs.

(6) In the future, weight proportions of hybrid nanoparticles in TES systems will have to be carefully selected by experimentalists so that the increment of the thermal conductivity will be much higher than that of the dynamic viscosity. Also, the effect of the magnetic field (Agrawal et al. 2020) on the PCM melting in TES applications could be investigated.

Nomenclature

c	Streaming speed [m.s^{-1}]
c_i	Discrete lattice velocity
c_p	Heat capacity[J.kg^{-1}.K^{-1}]
c_s	Speed of sound [m.s^{-1}]
d_{np}	Nanoparticle diameter [m]
d_{bf}	Molecular size of base fluid [m]
f	PDF for velocity field
f_l	Liquid fraction
Fo	Fourier number
g	PDF for temperature field
$\vec{g}$	Acceleration due to gravity [m.s^{-2}]
Gr	Grashof number
H	Height of cavity [m]
k	Thermal conductivity [W.m^{-1}.K^{-1}]
kb	Boltzmann constant
l	Length scale [m]
L	Length of cavity [m]
Nu	Nusselt number on hot surface
P	Pressure [kg.m^{-1}.s^{-2}]
Pe	Peclet number
Pr	Prandtl number
Ra	Rayleigh number
Ste	Stefan number
t	Time [s]
$\vec{u}$	Fluid velocity [m.s^{-1}]
$|\vec{u}_p|$	Brownian motion velocity [m.s^{-1}]
U_{max}	Maximum velocity in liquid phase
T	Dimensionless temperature
T_0	Dimensionless initial temperature of PCM
T_1	Dimensionless temperature of hot surface
X,Y	Dimensionless coordinates (x/l, y/l)
Z	Latent heat [J.kg^{-1}]

Greek symbols

α	Thermal diffusivity[m^2.s^{-1}]
β	Thermal expansion coefficient [K^{-1}]
φ	Volume fraction of nanoparticles
Δt	Lattice time step size
Δx	Lattice cell size
μ	Dynamic viscosity [kg.m^{-1}.s^{-1}]
ν	Kinematic viscosity [m^2.s^{-1}]
θ	Dimensionless time (Ste×Fo)
ρ	Density [kg.m^{-3}]
τ	Lattice relaxation time
ω	Weight function in LBM

Subscripts

av	Average
i, j	Directions
lbm	Lattice scale
nf	Nanofluid
np	Nanoparticles
max	Maximum
ref	Reference
fin	Conductive fins
bf	Base fluid

References

[1] Dhaidan, N.S. and Khodadadi, J.M., 2015. Melting and convection of phase change materials in different shape containers: A review. Renewable & Sustainable Energy Reviews, 43, pp. 449-477.

[2] Ho, C.J. and Viskanta, R., 1984. Heat transfer during inward melting in a horizontal tube. International Journal of Heat and Mass Transfer, 27(5), pp. 705-716.

[3] Hirata, T. and Nishida, K., 1989. An analysis of heat transfer using equivalent thermal conductivity of liquid phase during melting inside an isothermally heated horizontal cylinder. International Journal of Heat and Mass Transfer, 32(9), pp. 1663-1670.

[4] Hirata, T., Makino, Y. and Kaneko, Y., 1993. Analysis of natural convection melting inside isothermally heated horizontal rectangular cavity. Heat and Mass Transfer, 28, pp. 1-9.

[5] Hlimi, M., Hamdaoui, S., Mahdaouic, M., Kousksou, T., Msaad, A.A., Jamil, A. and Bouardi, A.E., 2016. Melting inside a horizontal cylindrical capsule. Case Studies in Thermal Engineering, 8, pp. 359-369.

[6] Gao, Z., Wu, H. and Yao, Y., 2019. Two-stage heat transfer characteristics of constrained melting inside an isothermally heated horizontal cylinder. International Journal of Thermal Sciences, 144, pp. 107-118.

[7] Imani, G., 2019. Lattice Boltzmann simulation of melting of a phase change material confined within a cylindrical annulus with a conductive inner wall using a body-fitted non-uniform mesh. International Journal of Thermal Sciences, 136, pp. 549-461.

[8] Dhaidan, N.S., 2021. Thermal performance of constrained melting of PCM inside an elliptical capsule of two orientations. Iranian Journal of Science and Technology, Transactions of Mechanical Engineering, 45, pp. 515-521.

[9] Ho, C.J., Wang, Z.C., Chen, R.H. and Lai, C.M., 2020. Conjugate heat transfer analysis of pcm suspensions in a circular tube under external cooling convection: wall conduction effects. Applied Sciences, 10(6), pp. 2034.

[10] Jourabian, M., Yuan, S., Zhang, J., Li, Y., Rabienataj Darzi, A.A. and Bayat, A. 2020. Melting within horizontal h-shaped enclosure with adiabatic curved boundary affected by inclination, mono/hybrid

nanofluids and fins. Journal of Enhanced Heat Transfer, 27(5), pp. 407-437.

[11] Mohammadifar, H., Sajjadi, H., Rahnama, M., Jafari, S and Wang, Y. 2021. Investigation of nanofluid natural convection heat transfer in open ended L-shaped cavities utilizing LBM. Journal of Applied and Computational Mechanics, 7(4), pp. 2064-2083.

[12] Agrawal, P., Dadheech, P.K., Jat, R.N., Nisar, K.S., Bohra, M. and Purohit, S.D., 2021. Magneto Marangoni flow of γ−Al2O3 nanofluids with thermal radiation and heat source/sink effects over a stretching surface embedded in porous medium. Case Studies in Thermal Engineering, 23, pp. 100802.

[13] Irwan M.A.M., Azwadi, C.S., Asako, Y. and Ghaderian, J. 2020. Review on numerical simulations for nano-enhanced phase change material (NEPCM) phase change process. Journal of Thermal Analysis and Calorimetry 141, pp. 669-684.

[14] Sciacovelli, A., Colella, F. and Verda, V. 2013. Melting of PCM in a thermal energy storage unit: Numerical investigation and effect of nanoparticle enhancement. International Journal of Energy Research, 37(13), pp. 1610-1623.

[15] Pahamli, Y., Hosseini, M.J., Ranjbar, A.A. and Bahrampoury, R. 2017. Effect of nanoparticle dispersion and inclination angle on melting of PCM in a shell and tube heat exchanger. Journal of the Taiwan Institute of Chemical Engineers, 81, pp. 316-334.

[16] Yadollahi Farsani R., Raisi, A. and Mahmoudi, A. 2019. Successive melting and solidification of paraffin–alumina nanomaterial in a cavity as a latent heat thermal energy storage. Journal of the Brazilian Society of Mechanical Sciences and Engineering, 41, pp. 368.

[17] Ouikhalfan, M., Sari, A., Chehouani, H., Benhamou, B. and Biçer. A. 2019. Preparation and characterization of nano-enhanced myristic acid using metal oxide nanoparticles for thermal energy storage. International Journal of Energy Research, 43(14), pp. 8592-8607.

[18] Xiong, T., Zheng, L. and Shah, K.W. 2020. Nano-enhanced phase change materials (NePCMs): A review of numerical simulations. Applied Thermal Engineering, 178, pp. 115492.

[19] Nizetic, S., Jurcevic, M., Arıcı, M., Arasu, V. and Xie, G. 2020. Nano-enhanced phase change materials and fluids in energy applications: A review. Renewable and Sustainable Energy Reviews, 129, pp. 109931.

[20] Yadav, C. and Sahoo, R.R. 2021. Effect of nano-enhanced PCM on the thermal performance of a designed cylindrical thermal energy storage system. Experimental Heat Transfer. 34(4), pp. 356-375.

[21] Chamkha, A.J, Doostanidezfuli, A., Izadpanahi, E. and Ghalambaz, M. 2017. Phase-change heat transfer of single/hybrid nanoparticles-enhanced phase-change materials over a heated horizontal cylinder confined in a square cavity. Advanced Powder Technology, 28(2), pp. 385-397.

[22] Ghalambaz, M., Doostani, A., Chamkha, A.J. and Ismael, M.A., 2017. Melting of nanoparticles-enhanced phase-change materials in an enclosure: Effect of hybrid nanoparticles. Internationa Journal of Mechanical Sciences, 134, pp. 85-97.

[23] C, K. and Zhao, Y. 2018. Effect of internal heat generation/absorption on Rayleigh-Bénard convection in water well-dispersed with nanoparticles or carbon nanotubes. International Journal of Heat and Mass Transfer, 127(Part A), pp. 1031-1047.

[24] Ma, Y., Mohebbi, R., Rashidi, M.M. andYang, Z. 2019. MHD convective heat transfer of Ag-MgO/water hybrid nanofluid in a channel with active heaters and coolers. International Journal of Heat and Mass Transfer 137, pp. 714-726.

[25] Costa, M., Oliva, A. and Pérez-Segarra, C.D. 1997. Three-dimensional numerical study of melting inside an isothermal horizontal cylinder. Numerical Heat Transfer Part A, 32(5), pp. 531-553.

[26] Gao, Z., Wu, H. and Yao, Y. 2019. Two-stage heat transfer characteristics of constrained melting inside an isothermally heated horizontal cylinder, International Journal of Thermal Sciences, 144, pp. 107-118.

[27] Esfe, M.H., Abbasian Arani, A.A., Rezaie, M., Yan, W.M. and Karimipour, A. 2015. Experimental determination of thermal conductivity and dynamic viscosity of Ag–MgO/water hybrid nanofluid, International Communications in Heat and Mass Transfer. 66, pp. 189-195.

[28] Zaraki, A., Ghalambaz, M., Chamkha, A.J., Ghalambaz, M. and De Rossi, D. 2015. Theoretical analysis of natural convection boundary layer heat and mass transfer of nanofluids: Effects of size, shape and type of nanoparticles, type of base fluid and working temperature. Advanced Powder Technology, 26(3), pp. 935-946.

[29] Nimmagadda, R. and Venkatasubbaiah, K. 2015. Conjugate heat transfer analysis of micro-channel using novel hybrid nanofluids

Al2O3+Ag/water. European Journal of Mechanics B/ Fluids, 52, 19-27.

[30] Ranga Babu, J.A., Kumar, K.K. and Srinivasa Rao S. 2017. State-of-art review on hybrid nanofluids, Renewable and Sustainable Energy Reviews, 77, pp. 551-565.

[31] Babar, H. and Ali, H.M. 2019. Towards hybrid nanofluids: Preparation, thermophysical properties, applications, and challenges. Journal of Molecular Liquids 281, pp. 598-633.

[32] Patel, H.E., Sundararajan, T., Pradeep, T., Dasgupta, A., Dasgupta, N. and Das, S.K. 2015. A micro convection model for the thermal conductivity of nanofluids. Pramana, 65, pp. 863-869.

[33] Ramazani Sarbandi, I., Taslimi, M.S. and Bazargan, V. 2020. Novel criteria for the optimum design of grooved microchannels based on cell shear protection and docking regulation: a lattice Boltzmann method study. SN Applied Sciences, 2, pp. 1823.

[34] Yazdi, H., Rahimian, M.H. and Safari, H. 2020. A lattice Boltzmann model for computing compressible two-phase flows with high density ratio. SN Applied Sciences, 2, pp. 83.

[35] Himrane, N., Ameziani, D.E. and Nasseri, L. 2020. Study of thermal comfort: numerical simulation in a closed cavity using the lattice Boltzmann method. SN Applied Sciences, 2, pp. 785.

[36] Khanafer, K., Vafai, K. and Lightstone, M. 2003. Buoyancy-driven heat transfer enhancement in a two-dimensional enclosure utilizing nanofluids, International Journal of Heat and Mass Transfer, 46, pp. 3639-3653.

[37] Chen, Z., Gao, D. and Shi, J. 2014. Experimental and numerical study on melting of phase change materials in metal foams at pore scale. International Journal of Heat and Mass Transfer, 72, pp. 646-655.

[38] Jourabian, M., Yuan, S., Zhang, J., Li, Y. and Rabienataj Darzi, A.A. 2020. Integrated influences of inclination, nanofluids, and fins on melting inside a horizontal enclosure with cross section of major circle sector. Heat Transfer Research 51(6), pp. 1-48.

[39] Rieger, H. and Beer, H. 1986. The melting process of ice inside a horizontal cylinder: effects of density anomaly. ASME, 108, pp. 166-173.

[40] Chen, G., Sun, G., Jiang, D. and Su, Y. 2020. Experimental and numerical investigation of the latent heat thermal storage unit with PCM packing at the inner side of a tube. International Journal of Heat and Mass Transfer 152, pp. 119480.

[41] Chen, W.Z., Yang, Q.S., Dai, M.Q. and Cheng, S.M. 1998. An analytical solution of the heat transfer process during contact melting of phase change material inside a horizontal elliptical tube. International Journal of Energy Research, 22(2), pp. 131-140.

[42] Fomin, S.A. and Wilchinsky, A.V. 2002. Shape-factor effect on melting in an elliptic capsule. International Journal of Heat and Mass Transfer, 45, pp. 3045-3054.

[43] Xie, H., Yu, W. and Chen, W. 2010. MgO nanofluids: higher thermal conductivity and lower viscosity among ethylene glycol-based nanofluids containing oxide nanoparticles. Journal of Experimental Nanoscience, 5(5), pp. 463-472.

[44] Mahmoodi, M. 2011. Numerical simulation of free convection of nanofluid in a square cavity with an inside heater. International Journal of Thermal Sciences, 50, pp. 2161-2175.

[45] Corcione, M. 2011. Empirical correlating equations for predicting the effective thermal conductivity and dynamic viscosity of nanofluids. Energy Conversion and Management, 52, pp. 789-793.

[46] Bayat, M., Faridzadeh, M.R. and Toghraie, D. 2018. Investigation of finned heat sink performance with nano enhanced phase change material (NePCM). Thermal Science and Engineering Progress, 5, pp. 50-59.